Amperomteric Ethanol Biosensor Based on Alcohol Dehydrogenase Immobilized at Poly-L-Lysine Coated Carminic Acid Functionalized Multiwalled Carbon Nanotube Film

Ya-Hui Ho, Arun Prakash Periasamy, and Shen-Ming Chen[*]

Department of Chemical Engineering and Biotechnology, National Taipei University of Technology, No.1, Section 3, Chung-Hsiao East Road , Taipei 106, Taiwan (ROC).
[*]E-mail: smchen78@ms15.hinet.net

Herein we report the preparation of stable aqueous dispersion of multiwalled carbon nanotubes (MWCNTs) using anthraquinone dye, carminic acid (CA) as a novel dispersing agent. The prepared CA functionalized MWCNT (CACNT) was characterized by scanning electron microscopy (SEM) and UV–vis absorption spectroscopy studies, which confirmed that MWCNTs are functionalized with CA. The prepared CACNTs were used to construct an amperometric ethanol biosensor based on ADH. The step-wise fabrication of the ADH/PLL/CACNT composite film on glassy carbon electrode (GCE) was monitored by electrochemical impedance spectroscopy (EIS). The electrostatic interactions between CACNT, PLL and ADH films add good stability to the immobilized ADH. Moreover, PLL and ADH are covalently immobilized at CACNT film surface. The covalent crosslinking occurs between the active amino groups of PLL and the carboxyl group of CA. Likewise the carboxyl groups of PLL undergoes crosslinking with the active amino group of ADH. We also confirmed from UV-visible spectroscopy results that ADH retains its native structure when it interacts with CACNT and PLL. The prepared ADH/PLL/CACNT composite film exhibits excellent amperometric response towards ethanol in the linear concentration range between 16.64-66.22 mM with a sensitivity of 0.158 $\mu A\ mM^{-1}\ cm^{-2}$. The composite film also detects ethanol present in red wine in good linear concentration range, which shows the practical applicability of this ADH based biosensor for ethanol quantification.

Keywords: Carminic acid, multiwall carbon nanotubes, poly-L-lysine, alcohol dehydrogenase, ethanol, electrocatalysis.

1. INTRODUCTION

The unique physical properties of multiwalled carbon nanotubes (MWCNTs) such as exceptional stability, high mechanical strength, and good electrical conductivity have made them a promising candidate for various applications [1]. Nevertheless, because of the hydrophobic nature of

MWCNTs and Van der Waals attractions between the nanotubes it is difficult to disperse the MWCNTs in aqueous and non-aqueous solvents. However, this shortcoming has been overcome by the attachment of functional groups at MWCNT walls through covalent and noncovalent approaches [2]. In order to functionalize MWCNT, noncovalent approaches are mostly preferred since this kind of approaches doesn't alter the electronic properties of MWCNT. The dispersing agents often used for noncovalent approaches are surfactants [3], polymers [4], DNA [5] and other biomoelcules [6]. However, the storage stability of these dispersions is of great concern, especially when biomolecules are used as dispersing agents. On the other hand, organic dyes have been widely employed as dispersing agents for MWCNTs since they possess good solubility in aqueous or organic solvents and they adsorb strongly at various substrates. Consequently, stable dispersion of MWCNT can be prepared by dispersing MWCNTs in organic dyes using simple ultrasonication treatments. The strong π-π stacking interactions between organic dyes and MWCNT help to maintain the stability of prepared MWCNT-organic dye aqueous dispersions. Moreover, this kind of strategy is advantageous since it is simple, economical, and the color variations of dye solutions could be visually observed and the MWCNT-dye adducts formed could be confirmed by several available spectroscopic and surface morphological studies [7].

Carminic acid (7-D-glucopyranosyl-3,5,6,8-tetrahydroxy-1-methyl-9,10-dioxo-9,10-dihydroanthracene-2-carboxylic acid or CA), is the active color ingredient of natural dye cochineal produced by Dactylopius coccus, a cochineal insect [8]. The chemical structure of CA is shown in scheme 1.
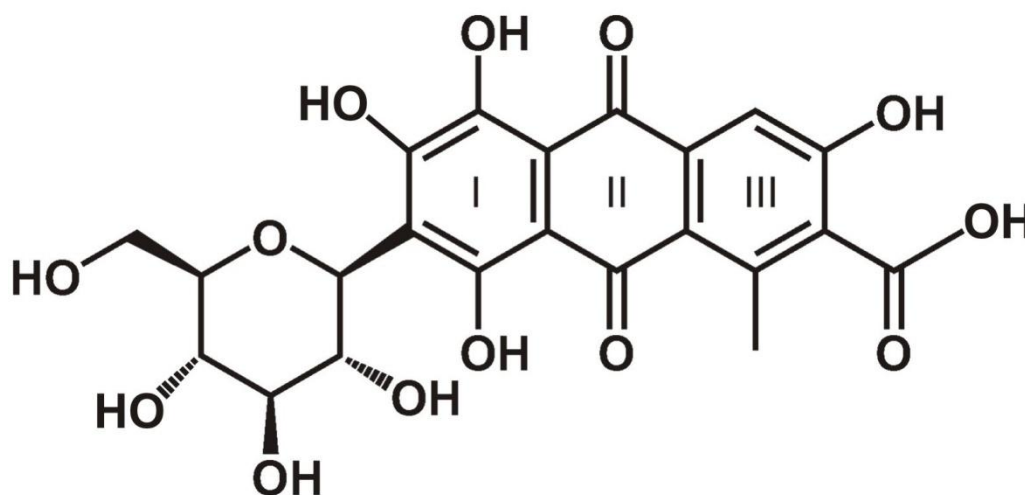
Scheme 1. Chemical structure of carminic acid (CA); the benzene rings are numbered as I, II and III.

CA is non-toxic, possess antitumor and antioxidant properties [9] and it has been used as a coloring agent in various food stuffs [10]. Moreover, CA has the ability to undergo strong interactions with biomolecules [11]. Besides, the redox properties of CA have made them a compound of great

electrochemical importance and so far the electrochemical [12, 13], impedance behavior [14] and spectroscopic analysis [15, 16] of CA have been reported by several research groups.

On the other hand, to achieve efficient ethanol quantification in clinical, food and beverage industries, alcohol dehydrogenase (ADH) based biosensors have been widely used. In ADH based ethanol biosensors irreversible oxidation of ethanol occurs in presence of both ADH and its cofactor nicotinamide adenine dinucleotide (NAD^+) at their close proximity [17]. The various immobilization matrices used in the past for ADH immobilization are ferrocene encapsulated ormosils [18], polyethylene glycol [19], colloidal gold [20], conducting polymers [21, 22], redox polymers [23] and multi-walled carbon nanotubes composite films [24-26].

In this work, without any tedious acid or chemical treatments we prepared a highly stable (up to four months), homogeneous MWCNT aqueous dispersion using anthraquinone dye, CA as the novel dispersing agent. The prepared MWCNT-CA aqueous dispersion (CACNTs) was casted on a glassy carbon electrode (GCE) surface and then coated with poly-L-lysine. This biocompatible PLL/CACNT film was used as a novel immobilization matrix for ADH. The electrostatic interactions between CACNT, PLL and ADH add good stability to the composite film. Moreover, PLL and ADH are covalently immobilized at CACNT film surface. We have described the fabrication, characterization and electrocatalytic applications of ADH/PLL/CACNT biosensor with selectivity and real sample studies.

2. EXPERIMENTAL

2.1 Reagents

CA was purchased from Sigma-Aldrich and used as received. PLL and ADH from Saccharomyces cerevisiae were obtained from Sigma. MWCNT with O.D. 10-15 nm, I.D. 2-6 nm, length 0.1-10 µm was obtained from Aldrich. The supporting electrolyte used for all experiments is 0.05 M pH 8.2 phosphate buffer solution (PBS) prepared using 0.05 M Na_2HPO_4 and NaH_2PO_4 solutions. All the reagents used were of analytical grade and doubly distilled water was used for the preparation of all aqueous solutions. Prior to each experiment, the experimental solutions were deoxygenated with pre-purified N_2 gas for 10 min and the N_2 tube was kept above the solutions to maintain an inert atmosphere.

2.2 Preparation of CACNTs

In order to prepare CACNTs, about 10 mg of MWCNT was added into 10 ml of 5 mM CA aqueous solution and the whole mixture was ultrasonicated for 1 h, until a homogeneous slight reddish-black dispersion was obtained. CACNT dispersion was then filtered and the solid material was subjected to several washings with water and over night dried at 50°C in an air oven. Thus obtained CACNTs were dissolved in aliquots of double distilled water and sonicated well to obtain a final concentration of 1 mg ml^{-1}. For comparison, without any CA addition 1 mg of as-received MWCNT

was dispersed in 1 ml of double distilled water and sonicated well. Hereafter, the term CNT used elsewhere in this paper will represent the non-functionalized MWCNT aqueous dispersion.

2.3 Fabrication of ADH/PLL/CACNT/GCE

Initially, 10 mg ml^{-1} ADH and 1 mg ml^{-1} PLL solutions were prepared separately in 0.05 M pH 8.2 PBS. The prepared ADH and PLL solutions were stored in refrigerator at 4 °C, when not in use. Prior to electrode modification, GCE surface was polished well on a clean Buehler polishing cloth using 0.05 μm alumina slurry. The polished GCE surface was washed with double distilled water, ultrasonicated for 10 min and finally dried at room temperature. 10 μl of CACNT aqueous solution was drop casted above the pre-cleaned GCE surface and dried at 30° C in air oven for 30 min. Then 20 μl of PLL (1 mg ml^{-1}) solution was drop casted above the CACNT film modified GCE and dried well at 30° C. Finally, 10 μl of ADH (10 mg ml^{-1}) solution was drop casted and dried for 30 min at 30° C. The prepared ADH/PLL/CACNT/GCE was then gently rinsed few times with doubly distilled water to remove the loosely bound ADH. The electrostatic interactions between the positively charged free −NH$_2$ group of PLL chains [27] and negatively charged carboxylic group (-COOH) of CA add stability to the composite film. Moreover, the positively charged PLL film can undergo electrostatic interactions with the negatively charged ADH layer (isoelectric point of ADH p*I*~6.8) [28]. Since PLL contains plentiful amino groups, it can react with carboxyl group of CA. Similarly, the carboxyl groups of PLL can interact with the active amino group of ADH. As a result, PLL and ADH are covalently immobilized at CACNT. This kind of combined electrostatic interactions and covalent crosslinking approaches can avoid the leaching of ADH from the PLL layer and thus it may provide good stability to the immobilized ADH. Ding et *al.* have reported the preparation of PLL/hydroxyapatite/CNT hybrid nanoparticles using the combined electrostatic interactions and covalent cross linking approaches [29]. For comparison, we prepared CACNT, PLL, ADH and PLL/CACNT films on GCE.

3. RESULTS AND DISCUSSIONS

3.1 CV studies at various film modified GCEs

Fig. 1 (A-C) shows the cyclic voltammograms obtained at various films modified GCEs in N$_2$ saturated 0.05 M pH 8.2 PBS at the scan rate of 50 mV s^{-1}. CA/GCE exhibits well defined quasi reversible redox peaks at a formal potential (E°′) of 0.475 V as shown in curve (a) of fig. 1 (A). The enlarged view of curve (a) is shown in fig. 1 (A) inset. In contrast, as shown in curve (b), CACNT/GCE exhibits enhanced redox peaks in the same potential window. During the forward scan, an anodic peak appears at 0.653 V, whereas two cathodic peaks appeared at 0.327 and 0.107 V in the reverse scan. The dramatic enhancement in the peak currents at CACNT/GCE indicates that CACNT effectively improves the electrode surface area and it promotes the electron transfer process. However, no redox peaks were observed at CNT/GCE in this potential window (Figure not shown). This result confirms that the redox process occurring at CACNT/GCE belongs to that of CA. In fig. 1 (B), no

significant redox peaks were observed at bare, ADH and PLL film modified GCEs, indicating their poor electron transfer ability (see curves (a-c)).
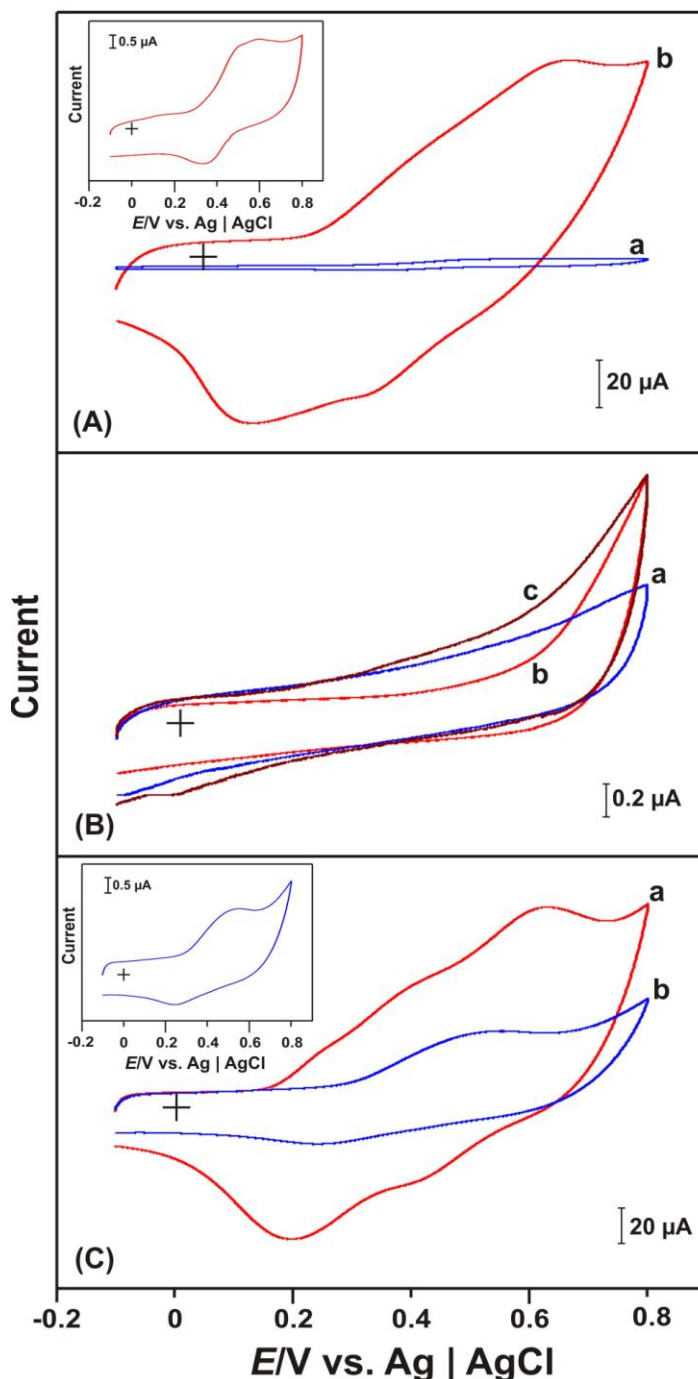
Figure 1. (A) Cyclic voltammograms obtained at (a) CA and (b) CACNT film modified GCEs in N$_2$ saturated 0.05 M pH 8.2 PBS at the scan rate of 50 mV s^{-1}. Inset is the enlarged view of curve (a). **(B)** Cyclic voltammograms obtained at (a) bare/GCE, (b) ADH, and (c) PLL film modified GCEs. **(C)** Cyclic voltammograms recorded at (a) PLL/CACNT, and (b) ADH/PLL/CACNT film modified GCEs. Inset is the enlarged view of curve (b). All the curves in fig. 1 (B) and (C) were recorded at similar conditions as fig. 1 (A).

As shown in curve (a) of fig. 1 (C), PLL/CACNT/GCE exhibits enhanced redox peaks. Compared with the cyclic voltammograms obtained at CACNT/GCE, the anodic peak shows 29 mV less positive potential shift, while the cathodic peaks show more positive potential shifts of 94 and 98 mV at PLL/CACNT/GCE, respectively. This can be due to the interactions between the oppositely charged CACNT and PLL films. On the other hand, as shown in curve (b) of fig. 1 (C), well-defined quasi reversible redox peaks with much lesser peak currents and more positive peak potential shifts were noticed at ADH/PLL/CACNT/GCE. In the forward scan, an anodic peak appears at an oxidation potential of 0.526 V. In the reverse scan unlike CACNT and PLL/CACNT/GCEs, only a single cathodic peak appears at 0.244 V. The formal potential (E°′) for this redox couple is 0.385 V. The decrease in peak currents and more positive redox peak potential shift indicates that ADH has been immobilized at ADH/PLL/CACNT/GCE. The reason for the decrease in the redox peak currents at ADH/PLL/CACNT/GCE may be due to the interaction between CA and the immobilized ADH. Sun et *al.* reported a similar voltammetric behavior for the interaction between CA and human serum albumin [11].

3.2 Different scan rate studies at ADH/PLL/CACNT composite film modified GCE
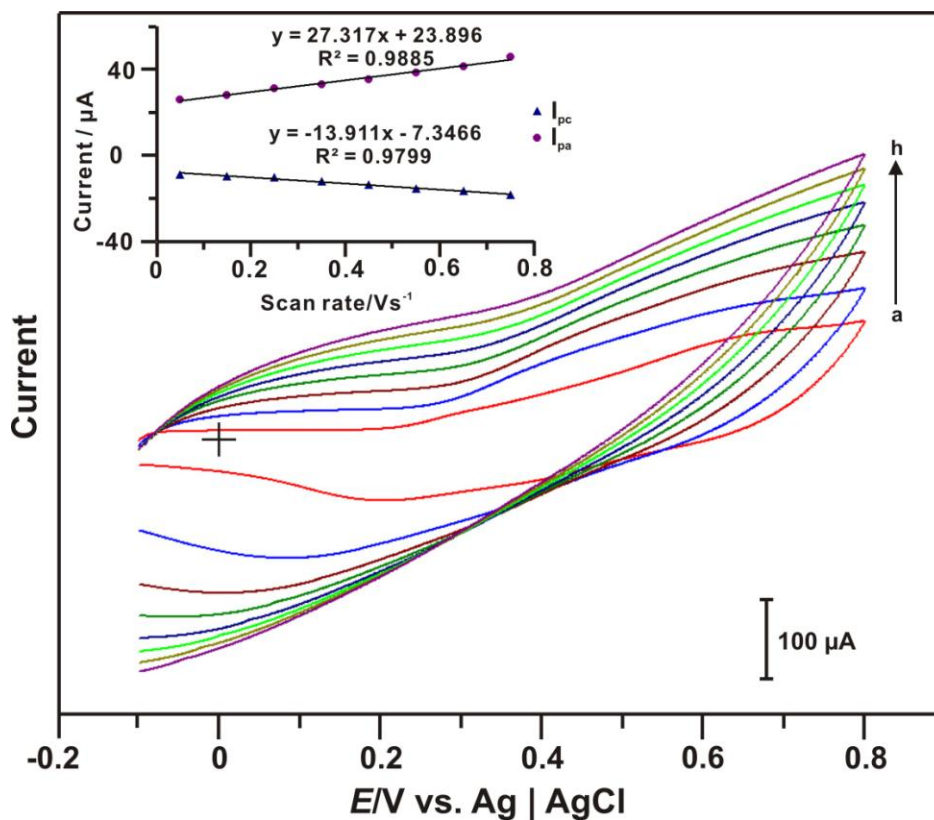
Figure 2. Cyclic voltammograms recorded at ADH/PLL/CACNT composite film modified GCE in N_2 saturated 0.05 M pH 8.2 PBS at different scan rates. The scan rates are (a) 50, (b) 150, (c) 250, (d) 350, (e) 450, (f) 550, (g) 650, and (h) 750 mV s^{-1}. The inset shows the plot of peak currents (I_{pa} and I_{pc}) vs. scan rate/Vs^{-1}.

Fig. 2 shows the cyclic voltammograms obtained at the ADH/PLL/CACNT composite film modified GCE in N_2 saturated 0.05 M pH 8.2 PBS at different scan rates. As shown in the inset, both I_{pa} and I_{pc} exhibit a linear dependence on scan rates between 50–750 mV s^{-1}, with R^2 = 0.9885 and 0.9799, respectively. This result indicates that the electrochemical redox process occurring at the composite film modified GCE is a surface confined process.

3.3 Influence of pH

Fig. 3 shows the effect of pH on the redox couple observed at ADH/PLL/CACNT composite film modified GCE in N_2 saturated different pH solutions. The composite film exhibits stable reversible redox peaks in the pH range between 1 and 13.
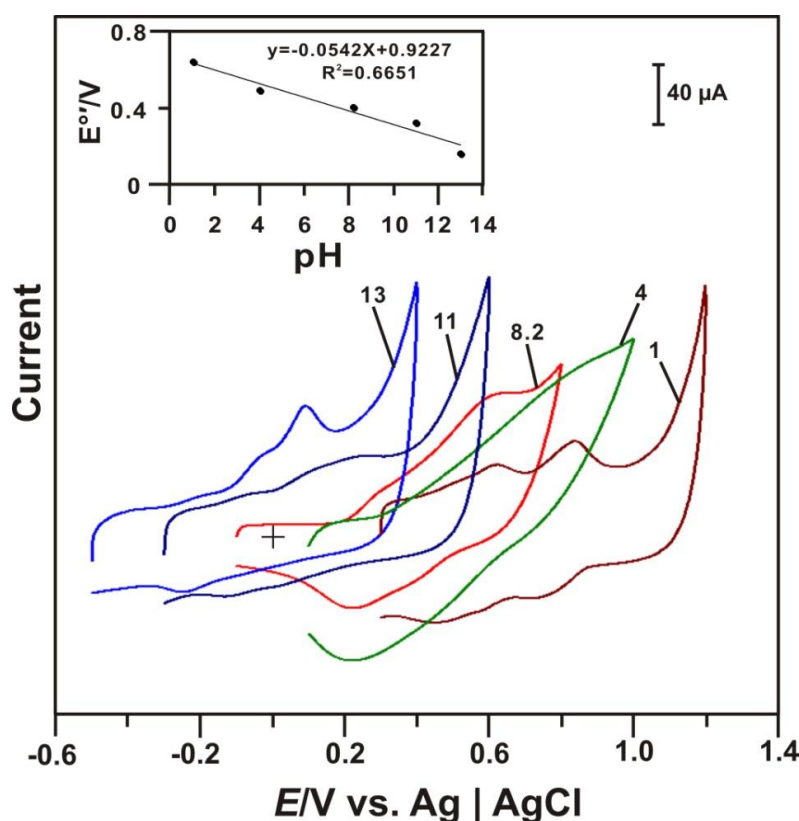
Figure 3. Cyclic voltammograms obtained at ADH/PLL/CACNT in N_2 saturated different buffer solutions with pH 1, 4, 8.2, 11 and 13, respectively. Scan rate = 50 mV s^{-1}. The inset is E°' vs. pH plot.

The influence of pH on E°' values are shown in fig. 3 inset. From the inset plot, it is apparent that E°' exhibit a linear dependence over pH. The slope value is 54 mV/pH, which is close to the theoretical slope value of 59 mV^{-1} pH for equal number of proton and electron transfer processes.

3.4 Surface morphological characterizations using SEM studies

Fig. 4 (a-e′) shows the SEM images of CNT, CACNT, ADH, PLL, and ADH/PLL/CACNT film coated ITOs at different magnifications. The SEM images of CNT displays agglomerated CNT bundles on the film surface, indicating the poor dispersing ability of CNTs in water (see fig. 4 (a-a')).
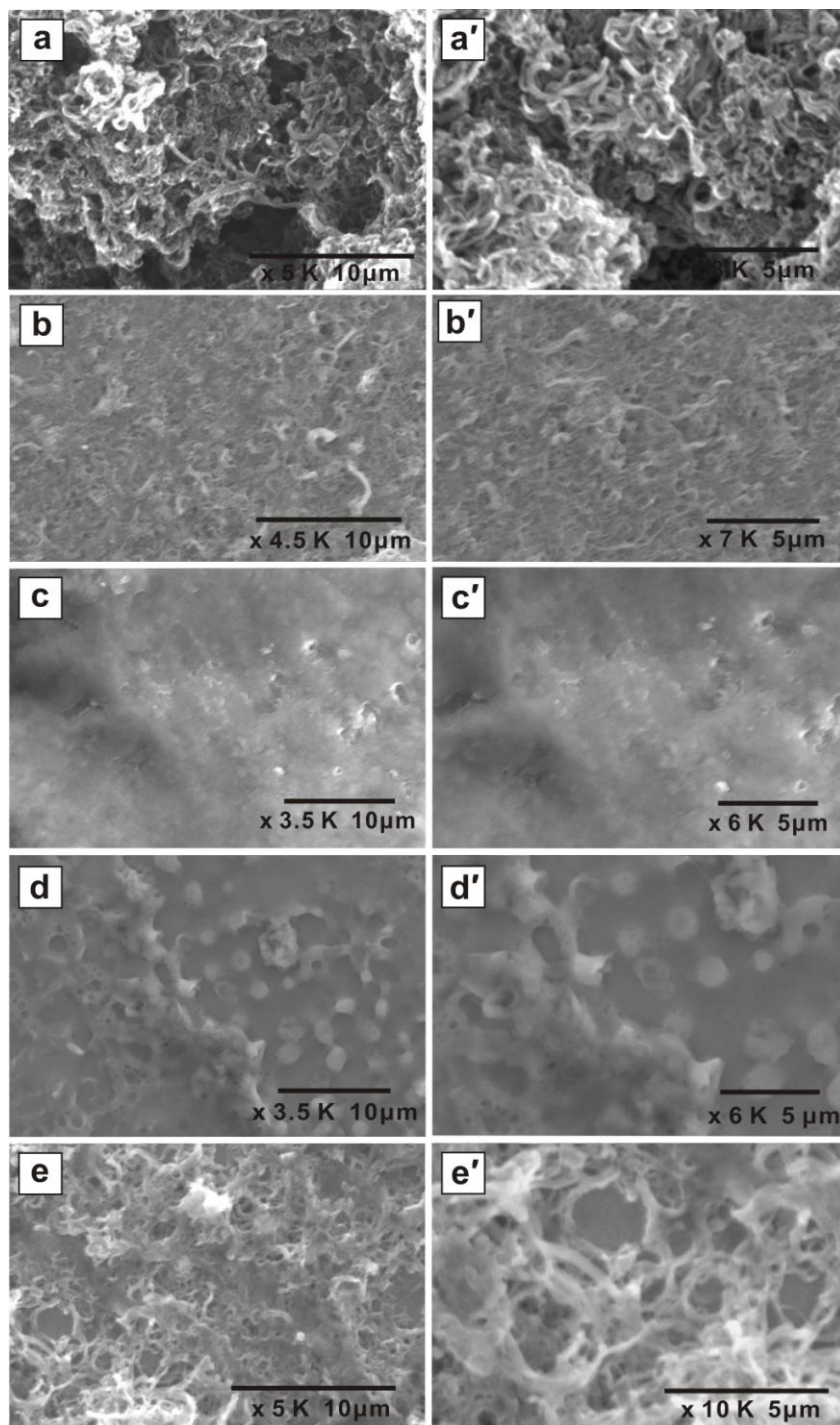
Figure 4. SEM images of (a) CNT, (b) CACNT, (c) ADH, (d) PLL, and (e) ADH/PLL/CACNT film coated ITOs at 10 µm magnifications. Fig. 4 (a′-e′) SEM images of above said films at 5 µm magnifications.

As shown in fig. 4 (b-b'), the SEM images of CACNT shows uniform well dispersed CACNTs, validating that CA is a good dispersing agent for MWCNTs. Whereas, ADH film displays thin uniform surface morphology (see fig. 4 (c-c')). The SEM images of PLL film coated ITO shows several small spherical beads like PLL structures (see fig. 4 (d-d'). In the SEM image of ADH/PLL/CACNT film, CACNTs are uniformly coated with bright PLL beads and ADH thin film (see fig. 4 (e-e')). This can be attributed to the strong electrostatic interactions between CACNT, PLL and ADH films. SEM studies thus reveal the discriminate surface morphology between different films and it validates that CACNT coated PLL film is efficient for ADH immobilization.

3.5 UV-visible absorption spectroscopy studies

Fig. 5 (a) shows the UV-visible absorption spectra of only CA, CNT and CACNT aqueous solutions along with ADH/PLL/CACNT mixture recorded in the wavelength range between 200–800 nm.
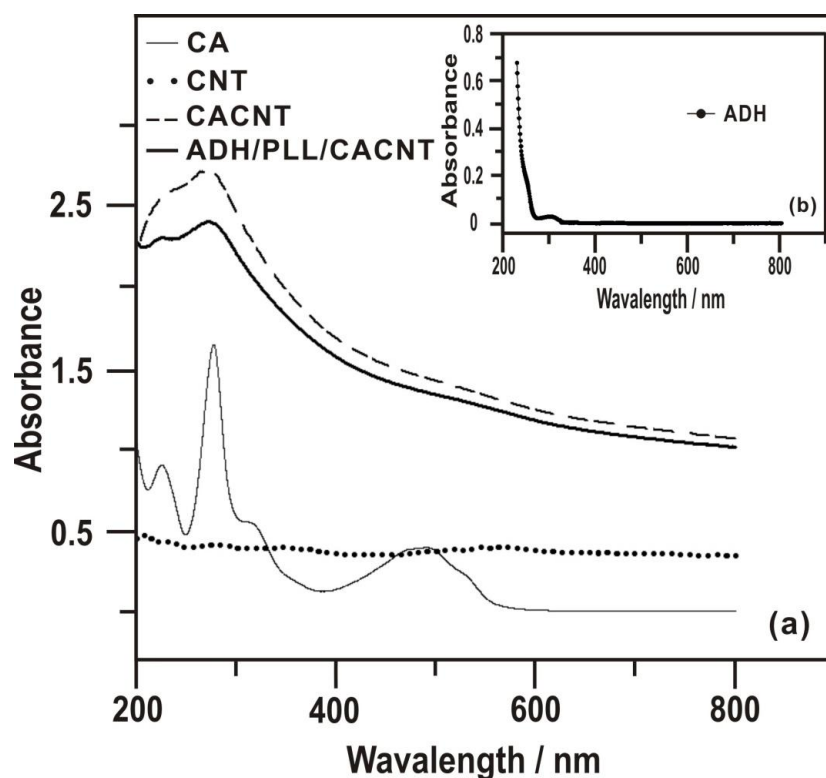
Figure 5. (a) UV-visible absorption spectra of only CA aqueous solution (thin line), CNT (dotted circles), and CACNT (dashed line) aqueous dispersions along with ADH/PLL/CACNT mixture (bold line) in the wavelength range between 200 and 800 nm. The inset (b) shows the UV-visible absorption spectra of only ADH aqueous solution (dotted circles with bold line).

The inset (b) in fig. 5 shows the UV-visible absorption spectra of only ADH aqueous solution recorded in the same wavelength range. In fig. 5 (a), UV-Visible absorption spectra of only CA

aqueous solution possess three characteristic absorption peaks at 232, 280 and 490 nm respectively. In particular, the absorbance maximum noticed at 490 nm for CA aqueous solution is close to the absorbance maximum of 492 ± 1 nm for 1×10^{-5} M CA aqueous solution [16]. However, CNT dispersion doesn't show any characteristic absorption peaks.

Compared with the UV-visible spectra of CA, UV-visible spectra of CACNT and the ADH/PLL/CACNT mixture exhibits identical characteristic CA absorption peaks at 232 and 280 nm indicating that MWCNTs are functionalized with CA.

Moreover, the absorption peak found at 280 nm in the UV-visible spectra of composite film is close to the absorption peak of ADH found at 279 nm, indicating that interaction of ADH with CACNT and PLL doesn't shift the absorption band of ADH. Therefore, the immobilized ADH should retain its native structure at the composite film.

3.6 EIS studies at different film modified GCEs

Fig. 6 (A) shows the real and imaginary parts of the impedance spectra represented as Nyquist plots (Z_{im} vs. Z_{re}) for bare and ADH film modified GCEs recorded in 0.05 M pH 8.2 PBS containing 5 mM $Fe(CN)_6^{3-/4-}$. Similarly, the Nyquist plots of ADH/PLL, CACNT, PLL/CACNT and ADH/PLL/CACNT film modified GCEs recorded under similar conditions are shown in fig. 6 (B). The inset in fig. 6 (B) shows the Randles equivalence circuit model fitted with the experimental data to obtain R_{et} and C_{dl} values for all films.

Generally, a semicircle portion of the Nyquist plot results from the parallel combination of R_{et} and C_{dl} resulting from electrode impedance [30]. In Fig. 6 (A), compared with bare GCE, an enlarged semicircle is observed in the Nyquist plot of ADH film modified GCE indicating the poor electron transfer ability of ADH/GCE. This may possibly be due to the repulsion between the negatively charged ADH film and negatively charged $Fe(CN)_6^{4-/3-}$ ions.

The R_{et} values observed at bare and ADH film modified GCEs are 600 Ω and 1540 Ω, respectively.

Whereas in fig. 6 (B), ADH/PLL/GCE possess a semicircle with much smaller diameter with an R_{et} value of 70 Ω, which is several folds smaller than the R_{et} value observed at ADH/GCE. This result indicates that interaction of negatively charged ADH with positively charged PLL film leads to faster electron transfer process at the ADH/PLL film surface.

On the other hand, no semicircles were found in the Nyquist plot of CACNT, PLL/CACNT and ADH/PLL/CACNT film modified GCEs. Instead they exhibit straight lines equivalence to the Wardburg impedance element in Randles circuit, indicating the mass transfer process. Moreover the linear portion of the Nyquist plot of these modified GCEs exhibits steady shifts after the sequential immobilization of PLL and ADH above the CACNTs, which may be attributed to the electrostatic interactions between these films.

The EIS results also confirmed that CACNT is highly conductive and both PLL and ADH films are well immobilized at the CACNTs.
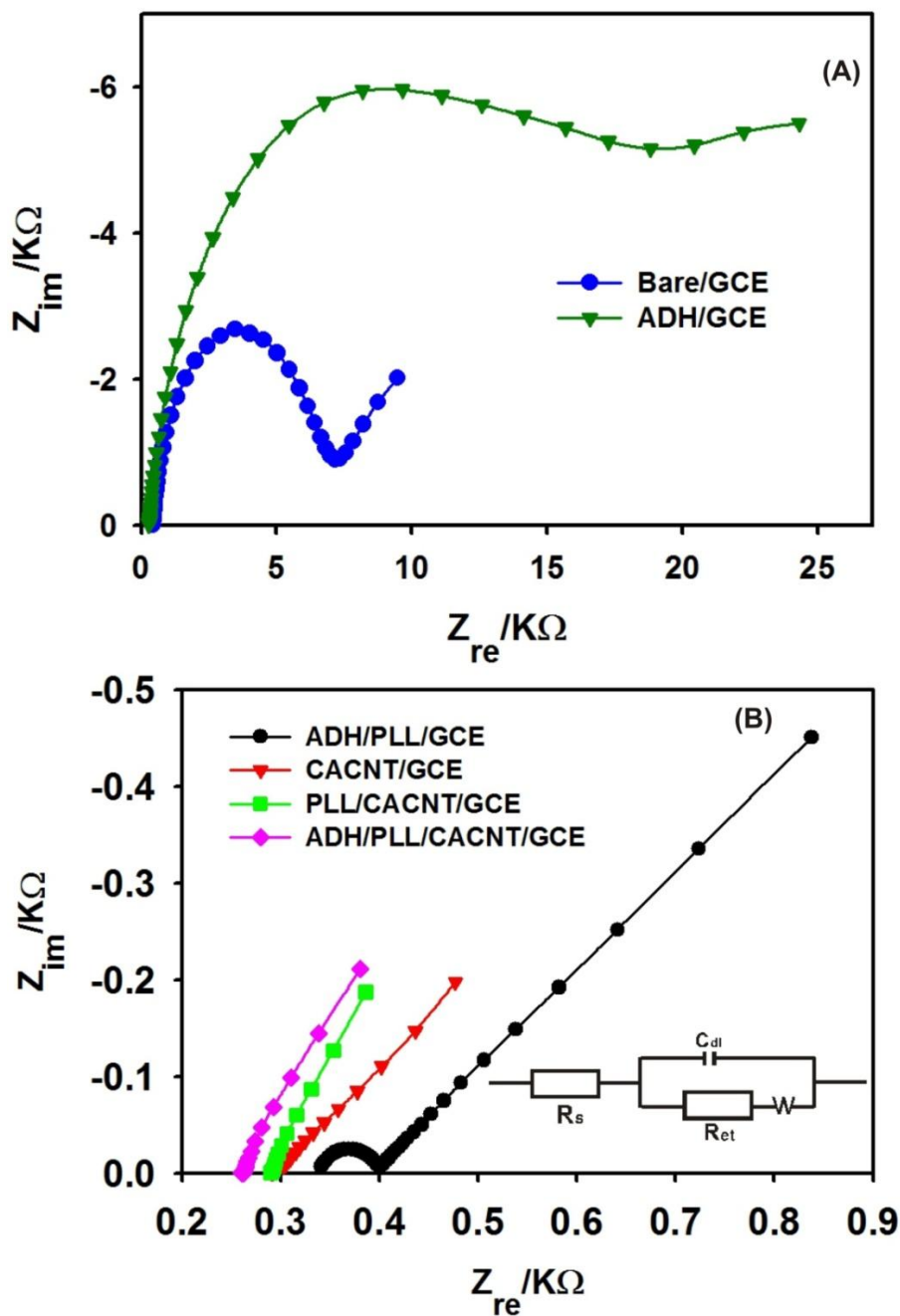
Figure 6. (A) EIS of bare and ADH/GCEs recorded in 0.05 M pH 8.2 PBS containing 5 mM Fe(CN)$6^{3-/4-}$. Amplitude: 5 mV, frequency: 100 mHz to 100 kHz. (B) EIS of ADH/PLL, CACNT, PLL/CACNT and ADH/PLL/CACNT film modified GCEs recorded at similar conditions as in fig. 6 (A). Inset in fig. 6 (B) shows the Randles equivalence circuit model fitted with the experimental data to obtain R_{et} values for all films.

3.7 Electrocatalysis of ethanol at the composite film modified GCE

In Fig. 7, the curves (a-h) shows the cyclic voltamograms obtained at ADH/PLL/CACNT composite film modified GCE for various ethanol concentration additions into N_2 saturated 0.05 M pH 8.2 PBS containing 10 mM NAD$^+$.
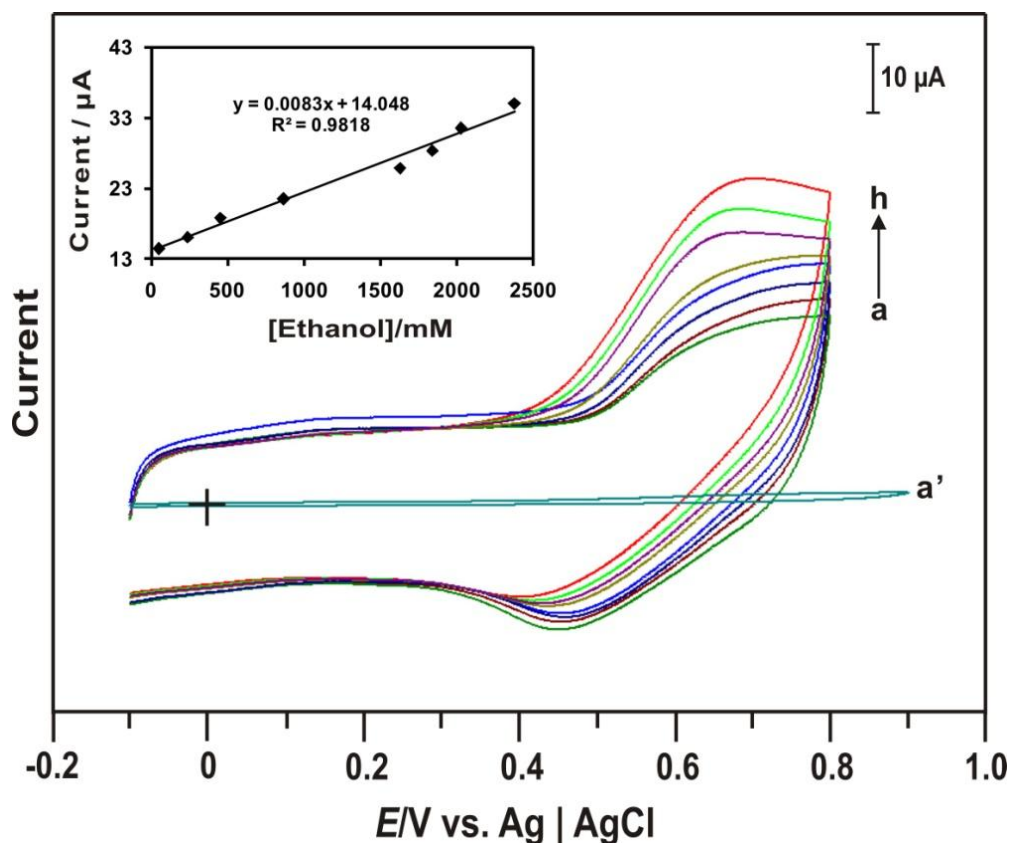
Figure 7. Cyclic voltammograms obtained at ADH/PLL/CACNT composite film modified GCE in the presence of (a) 49.5 mM, (b) 238.1 mM, (c) 454.5 mM, (d) 867.8 mM, (e) 1.63 M, (f) 1.85 M, (g) 2.03 M, and (h) 2.38 M ethanol in N_2 saturated 0.05 M pH 8.2 PBS containing 10 mM NAD^+ at 50 mV s^{-1} scan rate. (a′) Cyclic voltammograms obtained at bare/GCE in the presence of 2.38 M ethanol at similar conditions. Inset shows the linear dependence of I_{pa} on [Ethanol].

The potential range used is from -0.1 to 0.8 V. In fig. 7, ADH/PLL/CACNT film exhibits an enhanced electrocatalytic oxidation peak at 0.705 V for 49.5 mM ethanol. Since then with each ethanol concentration increments the oxidation peak current increased linearly between 49.50 mM–2.38 M (see curves (b-h)). However, no significant catalytic oxidation peaks are observed at bare GCE even in the presence of 2.38 M of ethanol (see (a') in fig. 7). Thus compared with bare GCE, the composite film modified GCE exhibits excellent electrocatalytic activity towards ethanol and it reduces the over potential for ethanol oxidation. The linear concentration range is between 49.5 mM–2.03 M ethanol and the sensitivity is 0.11 μA mM^{-1} cm^{-2}. Fig. 7 inset shows the linear dependence of I_{pa} on various ethanol concentrations. The linear regression equation is I (μA) = 0.0083 C (mM) + 14.048, R^2 = 0.9818.

3.8 Amperometric determination of ethanol at ADH/PLL/CACNT *composite film modified GCE*

Electrocatalytic oxidation of ethanol in acidic [31, 32], alkaline [33] or near neutral [34] pH has been studied widely using voltammetry technique for fuel cells, electrochemical sensors, and

biosensors applications. However, to achieve rapid response and wide linear range of ethanol detection at the modified electrode surface, amperometry technique can be more effective to probe the ethanol electrocatalytic oxidation reaction. Therefore in this study, we utilized amperometry technique to investigate the electrocatalytic oxidation at ADH/PLL/CACNT film in pH 8.2 PBS.
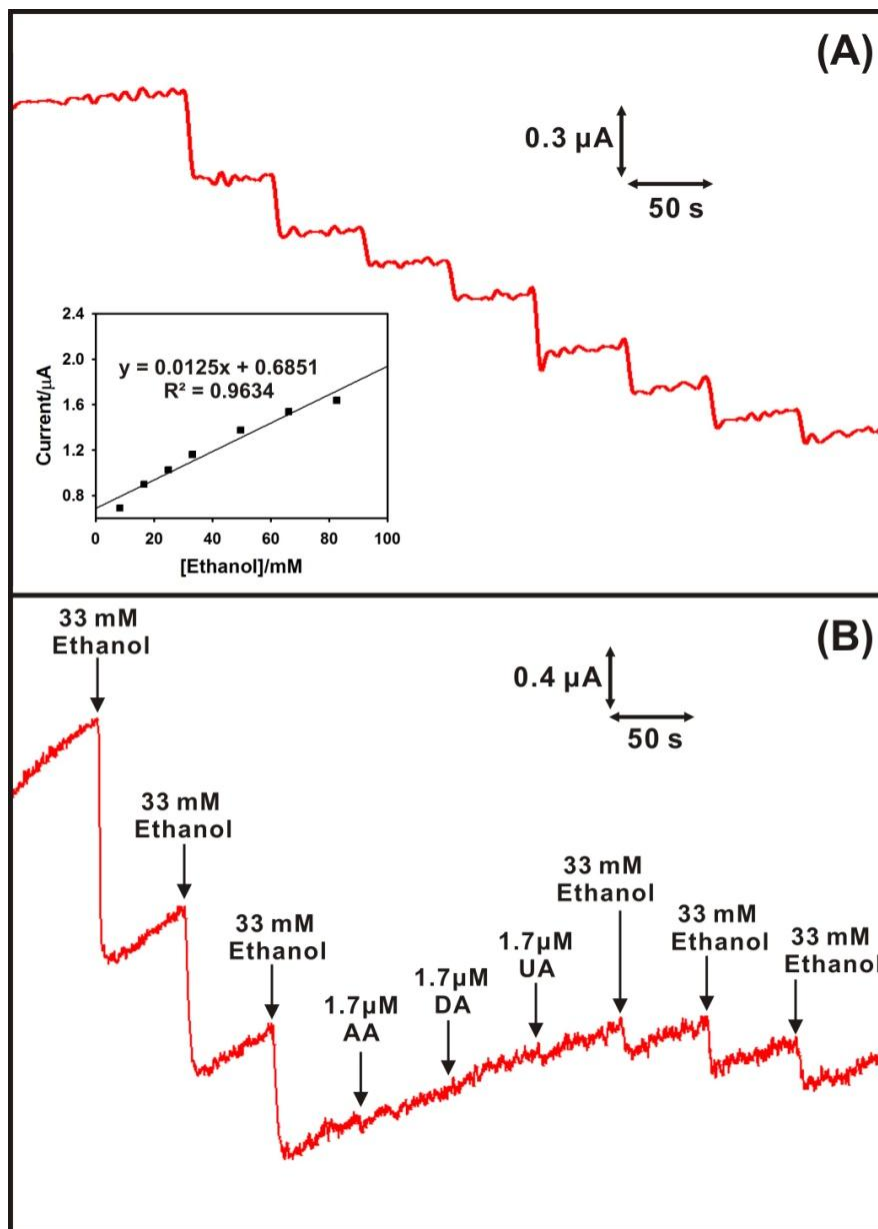
Figure 8. (A) Amperometric responses obtained at ADH/PLL/CACNT composite film modified GCE towards the addition of 8.33–259.7 mM ethanol into N_2 saturated 0.05 M PH 8.2 PBS containing 10 mM NAD^+. Applied potential: +0.7 V. The inset plot shows the linear dependence of I_{pa} on [Ethanol]/mM. **(B)** Amperometric responses obtained at ADH/PLL/CACNT composite film towards the successive additions of 33 mM ethanol both before and after each 1.7 μM of AA, DA and UA concentration additions. Other conditions are same as fig. 8 (A).

Fig. 8 (A) shows the amperometric responses obtained at ADH/PLL/CACNT composite film modified GCE towards various ethanol concentration additions into N_2 saturated 0.05 M pH 8.2 PBS containing 10 mM NAD^+. The electrode potential was kept constant at +0.7 V. Well defined amperometric responses were observed at the composite film for each ethanol concentration additions. The response time is 5 s. From the inset plot in fig. 8 (A), the linear ethanol concentration range, and sensitivity values are obtained as 16.64-66.22 mM, and 0.158 μA mM^{-1} cm^{-2}. The linear regression equation is I (μA) = 0.0125 C (mM) + 0.6851, R^2 = 0.9634. The amperometric study results revealed that composite film is efficient for ethanol oxidation.

The selectivity of the prepared ADH/PLL/CACNT composite film modified GCE has been investigated in the presence of common interferences such as ascorbic acid (AA), dopamine (DA) and uric acid (UA) using amperometric i-t curve studies. The results are shown in fig. 8 (B). As shown in fig. 8 (B), well defined amperometric responses were observed at ADH/PLL/CACNT composite film for each 33 mM of ethanol concentration additions. Whereas, no significant amperometric responses were observed at the composite film when each 1.7 mM of AA, DA and UA concentrations were added successively into the same supporting electrolyte solution. However, well defined amperometric responses were observed at the composite film immediately after each 33 mM ethanol concentration additions, indicating the good selectivity of the ADH/PLL/CACNT composite film towards ethanol in the presence of common interferences.

3.9 Real sample analysis

The practical applicability of ADH/PLL/CACNT composite film modified GCE has been investigated through real sample analysis using amperometric i-t curve studies. Commercially available red wine containing 12.5 % ethanol was purchased from local departmental store in Taipei, Taiwan. The red wine was diluted using 0.05 M pH 8.2 PBS. The working electrode potential was kept constant at +0.7 V. Fig. 9 shows the amperometric i-t curve recorded at ADH/PLL/CACNT composite film modified GCE towards various red wine (ethanol) concentration additions. The composite film exhibits well defined amperometric responses towards ethanol with a response time of 5 s.

From the inset plot the linear ethanol concentration range is observed to be between 30–180 mM. The linear regression equation is I (μA) = 0.0586 C (mM) + 2.1803, R^2 = 0.9879 and the sensitivity value is 0.74 μA mM^{-1} cm^{-2}, respectively. Real sample analysis results thus validate that composite film is efficient for ethanol determination and it can be employed for real sample applications.
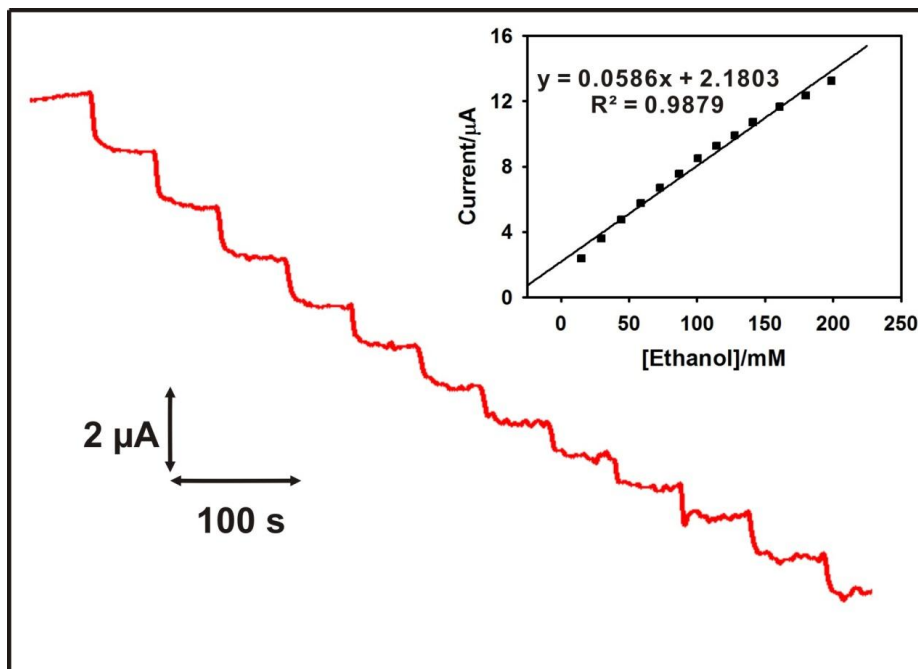
Figure 9. Amperometric responses obtained at ADH/PLL/CACNT composite film modified GCE towards the addition of 15 mM–199 mM ethanol containing red wine into N_2 saturated 0.05 M PH 8.2 PBS containing 10 mM NAD^+. Applied potential: + 0.7 V. The inset plot shows the linear dependence of I_{pa} on [Ethanol]/mM.

4. CONCLUSIONS

In this work, we report the preparation of a more stable aqueous dispersion of MWCNT using CA as the dispersing agent. The prepared CA functionalized CACNT dispersion possess good storage stability (up to four months) at room temperature. The CACNT modified electrode was used to construct an ADH based amperometric biosensor for ethanol quantification. The electrostatic interactions between the positively charged PLL and the negatively charged CACNT and ADH films add good stability to the immobilized ADH. Moreover, the crosslinking between the active amino groups of PLL and carboxyl groups of CA can avoid the leaching of ADH. Similarly, the cross linking between the carboxyl group of PLL and the free amino group of ADH also provide stability to the composite film. The developed ADH based biosensor possesses good biocompatibility, exhibits rapid response and promising electrocatalytic activity towards ethanol in good linear concentration range. The composite film has also been employed for the determination of ethanol from red wine. The present study validates that CACNT could be thus an interesting platform for immobilizing enzymes and for achieving faster electron kinetics and for selective biosensing applications.

References

1. D. Srivastava, C. Wei, *Appl. Mech. Rev.,* 56 (2003) 215.
2. D. Tasis, N. Tagmatarchis, A. Bianco, M. Prato, *Chem. Rev.,* 106 (2006) 1105.
3. I. Madni, C. Hwang, S. Park, Y. Choa, H. Kim, *Colloids and Surfaces A: Physicochem. Eng. Aspects*, 358 (2010) 101.
4. A. Liu, I. Honma, M. Ichihara, H. Zhou, *Nanotechnol.,* 17 (2006) 2845.
5. Z. Li, Z. Wu, K. Li, *Anal. Biochem.,* 387 (2009) 267.
6. S.E. Moulton, A.I. Minett, R. Murphy, K.P. Ryan, D. McCarthy, J.N. Coleman, W.J. Blau, G.G. Wallace, *Carbon,* 43 (2005) 1879.
7. W. Zhang, S.R.P. Silva, *Scr. Mater.,* 63 (2010) 645.
8. S. Gaweda, G. Stochel, K. Szacilowski, *J. Phys. Chem. C,* 112 (2008) 19131.
9. G.X. Li, Z.Q. Liu, D. Wu, *J. Phys. Org. Chem.,* 22 (2009) 883.
10. F.E. Lancaster, J.F. Lawrence, *J. Chromatogr. A,* 732 (1996) 394-398.
11. W. Sun, Y. Han, K. Jiao, *J. Serb. Chem. Soc.,* 71 (2006) 385.
12. T. Grygar, S. Kuckova, D. Hradil, D. Hradilova, *J. Solid. State. Electrochem.,* 7 (2003) 706.
13. A.D. Carbo, M.T.D. Carbo, M.C.S. Peris, J.V.G. Adelantado, F.B. Reig, *Anal. Bioanal. Chem.,* 375 (2003) 1169.
14. F. Am. Rashwan, *J. Appl. Sci.,* 2 (2005) 1595.
15. J.P. Rasimas, G.J. Blanchard, *J. Phys. Chem.,* 99 (1995) 11333.
16. M.V. Canamares, J.V.G. Ramos, C.D.S.S. Cortes, *Vib. Spectrosc.,* 40 (2006) 161.
17. A.M. Azevedo, D.M.F. Prazeres, J.M.S. Cabral, L.P. Fonseca, *Biosens. Bioelectron.,* 21 (2005) 235.
18. P.C. Pandey, S. Upadhyay, I. Tiwari and V.S. Tripathi, *Electroanal.,* 13 (2001) 820.
19. Q. Yao, S. Yabuki, F. Mizutani, *Sens. Actuators, B,* 65 (2000) 147.
20. Y. Liu, F. Yin, Y. Long, Z. Zhang and S. Yao, *J. Colloid Interface Sci.,* 258 (2003) 75.
21. K. Oshima, T. Nakamura, R. Matsuoka, T. Kuwahara, M. Shimomura and S. Miyauchi, *Synth. Met.,* 152 (2005) 33.
22. C. Jiang, H. Chen, J. Kong, *Electrochim. Acta,* 55 (2009) 142.
23. Y. Motoyama, N. Nakamura, H. Ohno, *Electroanal.,* 20 (2008) 923.
24. R.T. Kachoosangi, M.M. Musameh, I. Abu-Yousef, J.M. Yousef, S.M. Kanan, L. Xiao, S.G. Davies, A. Russell and R.G. Compton, *Anal. Chem.,* 81 (2009) 435.
25. C. Lee, Y. Tsai, *Sens. Actuators, B,* 138 (2009) 518.
26. M. Piao, D. Yang, K. Yoon, S. Lee and S. Choi, *Sensors,* 9 (2009) 1662.
27. Y. Zhang, J. Li, Y. Shen, M. Wang, J. Li, *J. Phys. Chem. B,* 108 (2004) 15343.
28. S. Liu, C. Cai, *J. Electroanal. Chem.,* 602 (2007) 103.
29. Y. Ding, J. Liu, X. Jin, H. Lu, G. Shen, R. Yu, *Analyst,* 133 (2008) 184.
30. S. Zong, Y. Cao, H. Jua, *Electroanal.,* 19 (2007) 841.
31. H. Li, D. Kang, H. Wang, R. Wang, *Int. J. Electrochem. Sci.,* 6 (2011) 1058.
32. Y. Umasankar, A.P. Periasamy, S.M. Chen, *Talanta,* 80 (2010) 1094.
33. R.M. Piasentin, E.V. Spinace, M.M. Tusi, A.O. Neto, *Int. J. Electrochem. Sci.,* 6 (2011) 2255.
34. A.P. Periasamy, Y. Umasankar, S.M. Chen, *Talanta,* 83 (2011) 930.